ACSNANO
www.acsnano.org
ARTICLE

Biotunable Nanoplasmonic Filter on Few-Layer MoS_2 for Rapid and Highly Sensitive Cytokine Optoelectronic Immunosensing

Younggeun Park,[†,§] Byunghoon Ryu,[†,§] Bo-Ram Oh,[†] Yujing Song,[†] Xiaogan Liang,[*,†] and Katsuo Kurabayashi[*,†,‡]

[†]Department of Mechanical Engineering and [‡]Department of Electrical Engineering and Computer Science, University of Michigan, Ann Arbor, Michigan 48109, United States

Supporting Information

ABSTRACT: Monitoring of the time-varying immune status of a diseased host often requires rapid and sensitive detection of cytokines. Metallic nanoparticle-based localized surface plasmon resonance (LSPR) biosensors hold promise to meet this clinical need by permitting label-free detection of target biomolecules. These biosensors, however, continue to suffer from relatively low sensitivity as compared to conventional immunoassay methods that involve labeling processes. Their response speeds also need to be further improved to enable rapid cytokine quantification for critical care in a timely manner. In this paper, we report an immunobiosensing device integrating a biotunable nanoplasmonic optical filter and a highly sensitive few-layer molybdenum disulfide (MoS_2) photoconductive component, which can serve as a generic device platform to meet the need of rapid cytokine detection with high sensitivity. The nanoplasmonic filter consists of anticytokine antibody-conjugated gold nanoparticles on a SiO_2 thin layer that is placed 170 μm above a few-layer MoS_2 photoconductive flake device. The principle of the biosensor operation is based on tuning the delivery of incident light to the few-layer MoS_2 photoconductive flake thorough the nanoplasmonic filter by means of biomolecular surface binding-induced LSPR shifts. The tuning is dependent on cytokine concentration on the nanoplasmonic filter and optoelectronically detected by the few-layer MoS_2 device. Using the developed optoelectronic biosensor, we have demonstrated label-free detection of IL-1β, a pro-inflammatory cytokine, with a detection limit as low as 250 fg/mL (14 fM), a large dynamic range of 10^6, and a short assay time of 10 min. The presented biosensing approach could be further developed and generalized for point-of-care diagnosis, wearable bio/chemical sensing, and environmental monitoring.

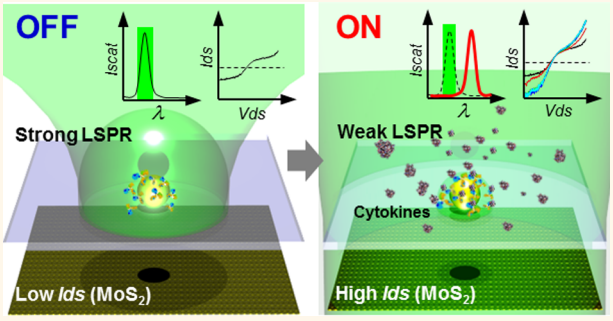

KEYWORDS: *nanoplasmonic filter, molybdenum disulfide, localized surface plasmon resonance, cytokine, immunosensing*

Cytokines are key biomolecules acting as mediators and modulators of the complex functional interactions and responses of the immune systems.[1−3] Quantifying cytokines allows monitoring of immune responses, providing clinically and immunologically useful information related to infectious diseases, cancer, autoimmune diseases, allergy transplantation, and drug discovery.[4] There has been an explosion in the use of cytokine-targeting immunotherapies for treating autoimmune diseases, infection,[5] cancer,[6] and other immune-related deficiencies.[7,8] Establishing a normal balance of a cytokine network in the host, these therapies have shown great promise for treating inflammatory diseases.[9,10] In treatment of a systemic inflammatory disorder, rapid and sensitive profiling of the cytokine-mediated immune response is required for realizing timely personalized immunomodulatory drug delivery to a critically ill patient. However, in conventional enzyme-linked immusorbent assay (ELISA) and bead-based immunoassay processes, the sensing signals are detected either by microplate readers or flow cytometers, which need very long (normally 3−8 h) and complicated assay processes. These assay techniques preclude researchers from analyzing inflammatory biomarker profiles and host-defense responses in real time during the course of disease development.[11−15] Recently, a great deal of research effort has been made to address this challenge. These efforts include nano/microscopic biosensing methods based on localized surface plasmon resonance (LSPR),[16−18] nano-enzyme-linked immunosorbent assay (Nano-ELISA),[19,20] microparticle control,[21] and so on. Never-

Received: February 19, 2017
Accepted: May 10, 2017
Published: May 10, 2017

DOI: 10.1021/acsnano.7b01162
ACS Nano 2017, 11, 5697−5705

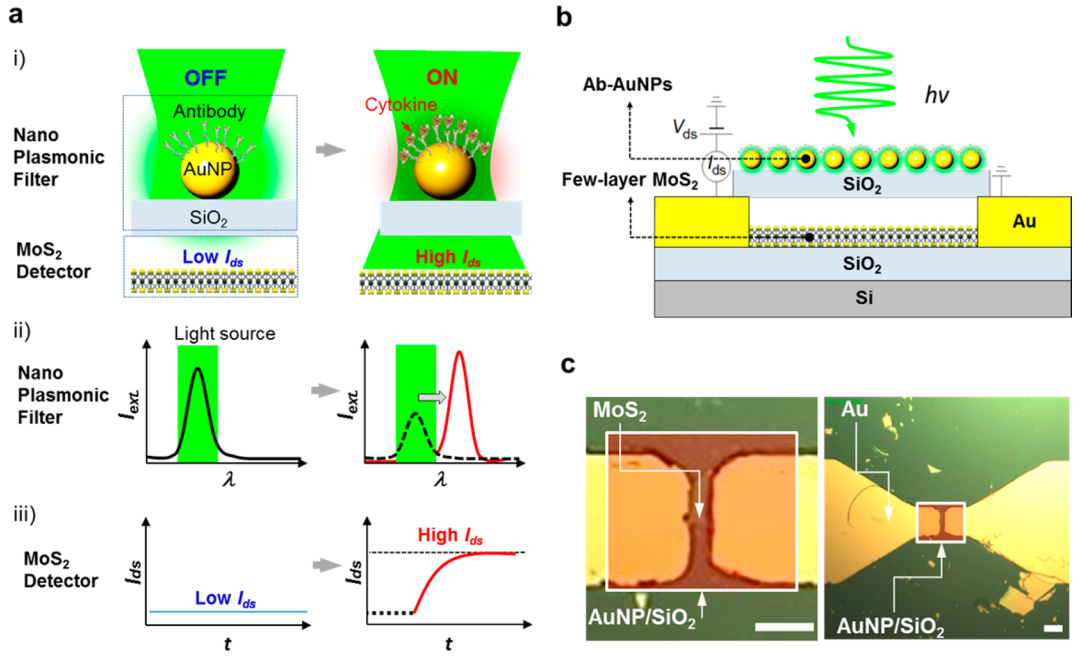

Figure 1. Biotunable nanoplasmonic optical filter on few-layer MoS_2 photodetector. (a) Schematic of decoupled nanoplasmonic optical filter on few-layer MoS_2 sensor for cytokine detection. (i) An antibody-attached plasmonic AuNP (d = 50 nm) resonates with incident light at λ = 532 nm. The resonance induces strong extinction around the Ab-AuNP on SiO_2. Due to the strong extinction, limited power density of incident light is delivered to the few-layer MoS_2 flake. The plasmonic resonance between the AuNP and the incident light results in lower photocurrent in MoS_2. When cytokines bind to the antibodies on the AuNP selectively, there is a change in the local refractive index. This local refractive index change decreases resonance between the cytokine-antibody-AuNP and the incident light. A larger portion of light-power density can be delivered to the MoS_2 film sensor. (ii) The extinction of the AuNP is matched to the incident light wavelength. Local refractive index change based on cytokines binding on the antibody-AuNP leads to a shift of the extinction peak. The extinction peak and wavelength of the incident light are no longer matched. (iii) Resonance between plasmonic extinction of the antibody-AuNP and the incident light source induces a decrease in the amount of the incident light detected in MoS_2. The extinction peak shift leads to a higher amount of the incident light detected. (b) Cross-sectional view of the structure of the decoupled nanoplasmonic optical filter and the few-layer MoS_2 photodetector together with electrical connections for device characterization. A few-layer MoS_2 (6.5 Å thick) flake is deposited on a degenerately doped silicon substrate with a 300 nm-thick SiO_2 layer. The substrate acts as a back gate. One of the gold electrodes acts as a drain, while the other, the source electrode, is grounded. (c) Optical microscope image of the decoupled AuNP/SiO_2 and MoS_2 nanoflake sensor (scale bar = 20 μm).

theless, these state-of-the-art methods still fall short of achieving high sensitivity and speed simultaneously in cytokine detection.

Owing to their attractive electronic/optical properties, large abundance, and compatibility to planar nanofabrication processes, atomically layered semiconducting materials, such as MoS_2, WSe_2, and WS_2, have recently garnered much attention as promising candidates for development of high-performance field-effect transistors (FETs) and other relevant nanoelectronic devices.[22−24] The transport characteristics of monolayer or few-layer MoS_2 FET channels are extremely sensitive to the external stimuli and can be exploited to make biosensors with high sensitivity and fast response speed.[25,26] Electrical response characteristics of such MoS_2 FET devices have been used to create ultrasensitive biosensors capable of detecting antigen−antibody binding events.[27,28] However, such purely electrical and electronic biosensors still suffer from degradation of detection stability and sensitivity over a long incubation time, which is attributed to ionic screening of electric field and unwanted short-circuit effects in an aqueous environment.[29−32] Specifically, the ions in an aqueous solution and other heterogeneous liquid components could result in serious shorting of electric circuits and distract electron current distribution in the presence of direct contact between the biomolecules and transistor regions. In this regard, alternative sensing mechanisms are needed to prevent the MoS_2-based sensing component from directly contacting with liquid reagents.

Here, we explore a cytokine biosensing approach based on a MoS_2 photoconductive device that is highly sensitive to light transmission through a biomolecule-capturing nanoplasmonic optical filter. In recent studies, photodetectors consisting of a MoS_2 layer-based photoconductive channel have been demonstrated as ultrasensitive photoresponse devices.[28,33,34] Our approach allows us to take full advantage of high photoabsorption coefficients resulting from the atomically layered structure of MoS_2 while avoiding the above-described contact of the photoactive structures with aqueous reagents. This study develops an integrated immunosensor device with a decoupled design that eliminates electron transfer between a nanoplasmonic structure and an atomically layered MoS_2 photodetector under light illumination to achieve highly sensitive, rapid, and stable cytokine detection. The nanoplasmonic optical filter of the device is an optically transparent SiO_2 layer (170 μm) coated with spherical gold nanoparticles (AuNPs; d = 50 nm). Light trapping by the AuNPs due to LSPR results in an efficient nano-optics filtering effect under resonant light illumination (λ = 532 nm). A LSPR shift induced by biomolecular surface binding causes a change in the light transmission characteristic of the filter. We find that the

DOI: 10.1021/acsnano.7b01162
ACS Nano 2017, 11, 5697−5705

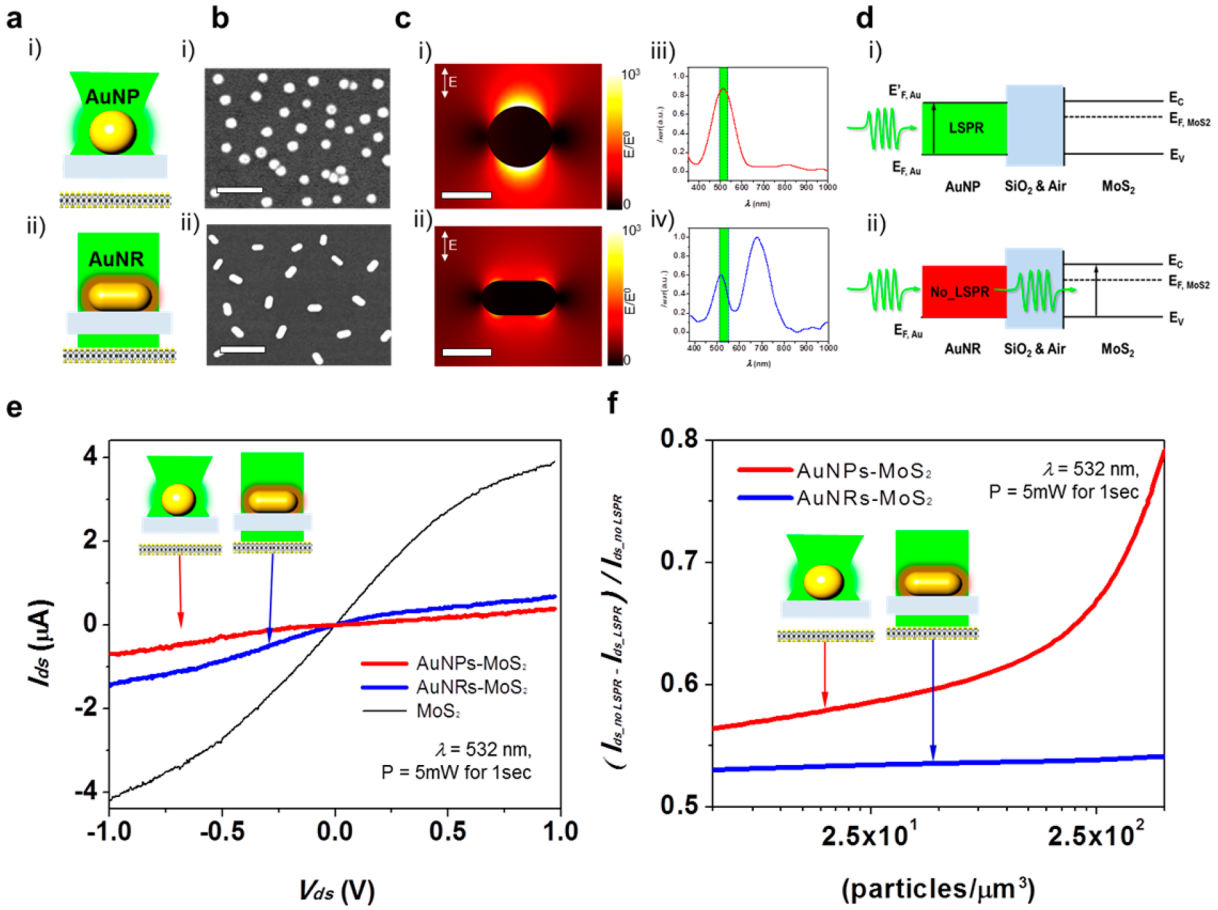

Figure 2. LSPR-induced selective photoenhancement effect on AuNP nanoplasmonic optical filter and MoS_2 photodetector. (a) Plasmonic resonance induces optical filtering effects. The selective photodetection based on plasmon resonance is verified by comparison between (i) AuNP (d = 50 nm) and (ii) AuNR (d/l = 40/68 nm)-coated SiO_2 layers. (b) SEM image of AuNP and AuNR arrays on SiO_2 (scale bar = 500 nm). (c) Calculated electric-field distribution based on FEA reveals high extinction for (i) the AuNP and lower extinction for (ii) the AuNR with incident light at λ = 532 nm (scale bar = 50 nm). Extinction peak of (iii) the AuNP located at ~532 nm and extinction peaks of (iv) the AuNR located at 530 and 670 nm. Under the light source at λ = 532 nm, the AuNP leads to lower photocurrent. The AnNR array results in higher photocurrent. (d) Schematic of the optical filtering mechanism through the SiO_2 layer between the AuNP (or AuNR) metal nanostructure and the atomically layered MoS_2 (semiconductor) without bandgap bending: (i) A LSPR mode in the metal nanostructure enables filtering of the incident light, and (ii) no LSPR leads to transmission of photons to the atomically layered MoS_2. (e) Comparison of photocurrent between the AuNP and the AuNR, (f) nanoplasmonic filtering enhancement ($(I_{ds\_no\ LSPR} - I_{ds\_LSPR})/I_{ds\_no\ LSPR}$) as a function of the density of plasmonic particles in the atomically layered MoS_2.

biosensor device enables us to detect a pro-inflammatory cytokine, IL-1β, at a concentration as low as 250 fg/mL (14 fM) with a sampling-to-answer time of ~10 min. We anticipate that such a LSPR-modulated optoelectronic biosensor can find a wide range of applications, including point-of-care disease diagnosis and environmental monitoring.

RESULTS AND DISCUSSION

Figure 1 illustrates the underlying concept of hybrid integration of a AuNP-SiO_2 nanoplasmonic filter layer and a few-layer MoS_2 photoconductive flake on a common device platform for cytokine detection. The AuNPs (d = 50 nm) on the SiO_2 layer are coated with antibodies (Ab) specifically targeting IL-1β. In the absence of the targeted cytokine (IL-1β) molecules, the Ab-coated AuNPs block incident light at λ = ~532 nm as a result of the LSPR effect ("OFF" mode). In the OFF mode, light transmission through the SiO_2 layer becomes weak, keeping incident light from reaching the underlying few-layer MoS_2 photoconductive flake. Now, binding of IL-1β molecules onto the Ab-coated AuNP surfaces shifts the plasmonic resonance wavelength, owing to a change in the local refractive index near the AuNP surfaces.[16−18] A larger fraction of the incident photons then transmits through the SiO_2 thin layer and reaches the underlying MoS_2 photoconductive flake ("ON" mode). The ON mode results in a red shift of the extinction spectrum peak of the AuNP-SiO_2 nanoplasmonic filter layer, thus leading to an increased photoconduction of the MoS_2 flake. The photoconduction of the device is determined by the cytokine concentration of a sample solution deposited on the device surface covered with the AuNP-SiO_2 thin layer. Obtaining a correlation between the photoconduction change and the cytokine concentration allows highly sensitive quantification of IL-1β.

Figure 1b shows a cross-sectional view of the whole decoupled device architecture, where the nanoplasmonic filter and few-layer MoS_2 flake are physically decoupled by an intermediate SiO_2 thin layer with an air gap. This decoupled architecture ensures nonphysical contact between the plasmonic nanostructure and semiconducting structures, while other previous device structures incorporated a metal/semi-

DOI: 10.1021/acsnano.7b01162
ACS Nano 2017, 11, 5697−5705

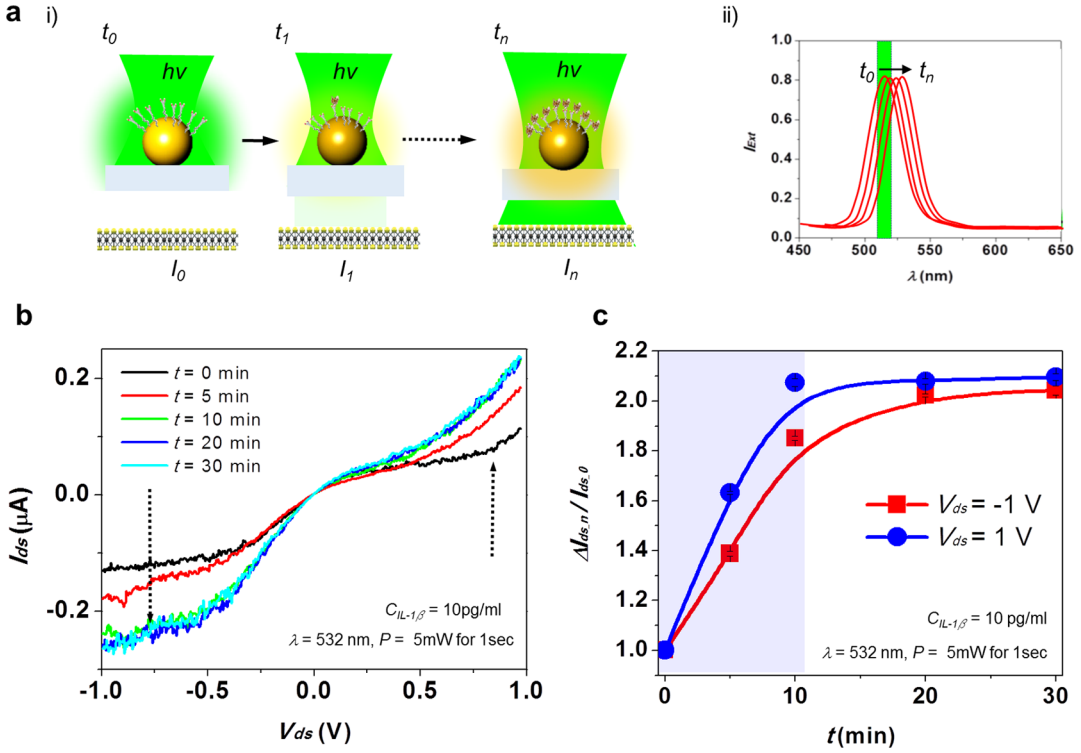

Figure 3. Rapid detection performance of biotunable nanoplasmonic optical filter on few-layer MoS_2 photodetector. (a) IL-1β surface binding effect on phototransmission of nanoplasmonic optical filter over time: (i) The increasing number of IL-1β bound to the antibody-coated AuNP causes shifts of the AuNP LSPR extinction peak and thus increases the phototransmission incident light through the nanoplasmonic optical filter; (ii) the AuNP extinction spectrum experiences red-shifts over time during IL-1β surface binding incubation. An increase of IL-1β surface binding-induced phototransmission leads to a high level of photocurrent in the few-layer MoS_2 photodetector (green line: incident light spectrum; and red curve: nanoplasmonic optical filter extinction spectrum). (b) I_{ds} *vs* V_{ds} curves of the few-layer MoS_2 photodetector at different IL-1β surface binding incubation time points for a fixed IL-1β concentration of $C_{IL\text{-}1\beta}$ = 10 pg/mL. Each curve is obtained under illumination of light at λ = 532 nm, P = 5 mW for 1 s, and (c) photocurrent variation ($\Delta I_{ds\_t}/I_{ds\_0}$) over time during incubation process at V_{ds} = 1.0 and −1.0 V for $C_{IL\text{-}1\beta}$ = 10 pg/mL.

conductor interface.[35] In general, at the metal/semiconductor interface, it is well-known that electron transfer takes place between the plasmonic nanostructure and the few-layer MoS_2 flake due to band gap bending. The metal/semiconductor contact device architecture allows direct interaction between plasmonic nanostructure/few-layer MoS_2 and biomolecules in an aqueous solution, which leads to nonuniform surface charge distribution and signal instability. In our decoupled architecture, electron transfer causing irradiative plasmon decay is minimized. As such, radiative decay of plasmons in the nanoplasmonic structure only determines the sensitivity of few-layer MoS_2 while maintaining high stability of the electrical signal.

We first tested the impact of LSPR on the nanoplasmonic filtering effect of our device using gold nanospherical particles (AuNPs) and gold nanorod particles (AuNRs) on a SiO_2 thin layer. The SiO_2 layer was placed on two electrodes adjacent to a few-layer MoS_2 photoconductive film, which were connected to electronics used to characterize the device. One of the gold electrodes acting as a drain was connected to a voltage source, while the other, the source electrode, was grounded (Figure 1b, Figure 2, and Methods and Experimental Section). The testing structures were prepared by attaching nanoparticles to a 3-aminopropyl triethoxysilane (APTES)-functionalized SiO_2 thin layer with an amino functional group. The resulting AuNP and AuNR structures on the SiO_2 thin layer revealed uniform color over ∼5 mm^2 area samples, which suggested uniform distribution of the nanoparticles on the surface. The morphology and optical property of each testing structure were analyzed by scanning electron microscopy (SEM) and ultraviolet−visible (UV−vis) spectrometer. We verified that a monolayer of AuNPs or AuNRs was uniformly distributed on the SiO_2 thin layer without aggregations for each structure. Same particle density of the AuNPs and AuNRs (Figure 2b, $d_{particle}$ = ∼125 particles/μm^3) were tested.

Our system used a visible laser light source at λ = 532 nm ±10 nm. The fabricated few-layer MoS_2 photoconductive flake shows sufficient photoresponsivity at this wavelength (Figure S1). The wavelength λ = 532 nm lies in a biologically benign optical band. The MoS_2 flake exhibits higher photoresponsivity at shorter wavelengths in the UV region, but UV light is often harmful to biological systems. The AuNPs (d = 50 nm) exhibit a strong LSPR peak at this wavelength, while the primary (longitudinal) plasmonic resonance peak of the AuNRs (d = 40 nm and l = 68 nm) lies at λ = 680 nm, where the MoS_2 flake experiences a significant reduction of photoresponsivity. Choosing the excitation light source wavelength λ = 532 nm also brings a practical benefit that enables us to use AuNPs for the nanoplasmonic optical filter of our device rather than AuNRs. AuNPs are more readily commercially accessible than AuNRs because of their much simpler synthesis requirements and cost effectiveness.

Calculated electric-field distributions around AuNP and AuNR show the high extinction in AuNP (Figure 2c). Then,

DOI: 10.1021/acsnano.7b01162
ACS Nano 2017, 11, 5697−5705

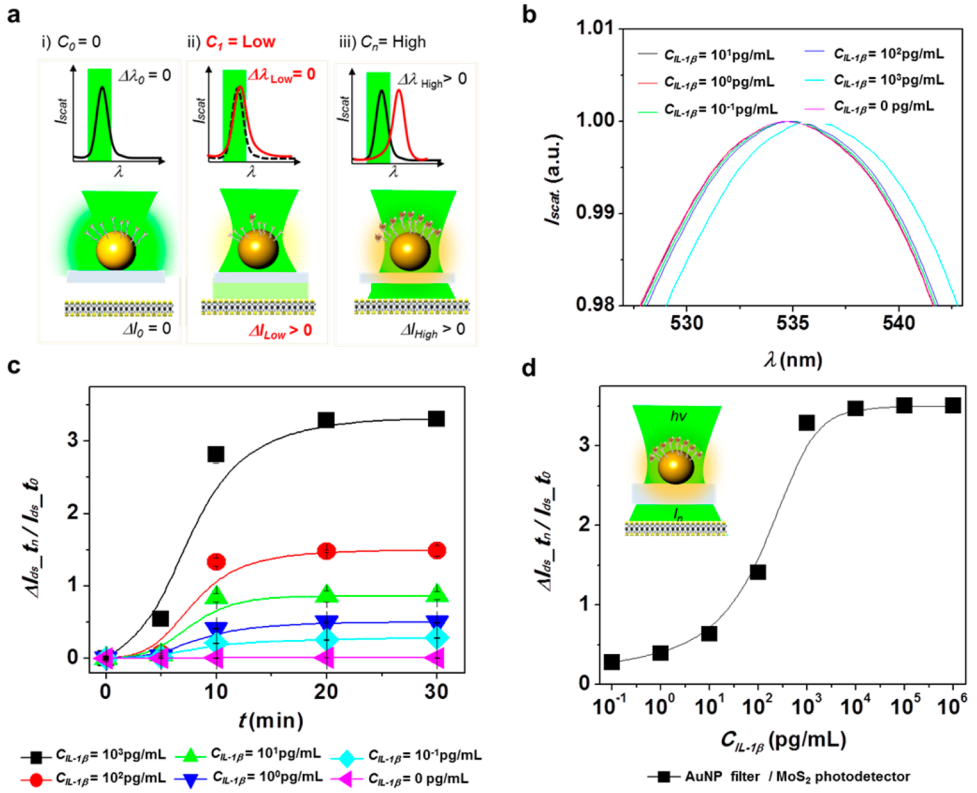

Figure 4. IL-1β Sensitivity of biotunable nanoplasmonic optical filter on few-layer MoS_2 photodetector. (a) Illustration of highly sensitive IL-1β detection using few-layer MoS_2: (i) At a cytokine (IL-1β) free environment (C_0 = 0), no peak shift of the AuNP LSPR spectrum (represented by the scattering light spectrum I_{scat} here) or no photocurrent change is observed; (ii) at a low concentration of IL-1β (C_1), a weak change of local refractive index at the AuNR surface leads to a I_{scat} peak shift hardly measurable by a photospectrometer ($\Delta\lambda_{low} \sim 0$), while the photocurrent change ($\Delta I_{low} > 0$) is detectable with the high-sensitivity few-layer MoS_2 photodetector; and (iii) at a higher concentration of IL-1β (C_n), both the I_{scat} peak shift ($\Delta\lambda_{high} > 0$) and the photocurrent changes ($\Delta I_{high} > 0$) are highly noticeable. (b) LSPR spectra of AuNP-coated SiO_2 surface at $C_{IL\text{-}1\beta}$ ranging from 0.1 pg/mL to 1 ng/mL. (c) Photocurrent variation ($\Delta I_{ds\_t}/I_{ds\_0}$) during IL-1β surface binding incubation for different $C_{IL\text{-}1\beta}$ values. Each curve is obtained under photoillumination at λ = 532 nm, P = 5 mW for 1 s, and (d) standard curve of photoelectronic cytokine immunobiosensor incorporating biotunable nanoplasmonic optical filter on a few-layer MoS_2 photodetector.

we hypothesized that the plasmonic filtering effect would cause the AuNPs to yield a lower photocurrent signal in the few-layer MoS_2 flake than the AuNRs (Figure 2d). Our photoconduction experiment was performed for devices incorporating the testing structures above (Figure 2e). The test obtained a photocurrent of I_{ds} = 0.21 μA at a drain−source voltage of V_{ds} = 1.0 V and I_{ds} = −0.7 μA at V_{ds} = −1.0 V with the AuNPs, whereas I_{ds} = 0.75 μA at V_{ds} = 1.0 V and I_{ds} = −1.5 μA at V_{ds} = −1.0 V with the AuNRs. These experimental results verified our hypothesis, indicating more significant plasmonic filtering effect with the AuNPs than with the AuNRs, which proves that strong extinction-based resonance between plasmonic nanoparticle and incident light determines the performance of the nanoplasmonic filter. In addition, we controlled the density of AuNPs on SiO_2, expecting that it would tune the filtering intensity under the resonance condition. Here, we prepared testing structures with 6 different densities of AuNPs and AuNRs: ∼5, ∼25, ∼50, ∼125, ∼250, and ∼1000 particles/μm^3. These specimens showed a narrow size distribution regardless of their density on the substrate. This narrow size distribution minimized LSPR spectrum broadening for all the structures for both AuNPs and AuNRs. The extinction spectrum peak locations were consistent across the specimens regardless of the nanoparticle density except for ∼1000 particles/μm^3. We find a density higher than ∼1000 particles/μm^3 causes interparticle plasmonic coupling induced by an increase in the refractive index (Figures S2 and S3), which results in a broader spectrum of the extinction peak. To quantify the plasmonic filtering effect, we defined the nanoplasmonic filtering enhancement as $(I_{ds\_no\ LSPR} - I_{ds\_\ LSPR})/I_{ds\_no\ LSPR}$, where $I_{ds\_\ LSPR}$ and $I_{ds\_no\ LSPR}$ are the photocurrent with and without plasmonic nanoparticles on the SiO_2 thin layer, respectively. The nanoplasmonic filtering enhancement with the nanoparticle density shown in Figure 2f is further evidence supporting the mechanism of our nanoplasmonic filter. The nanoplasmonic filtering variation from AuNPs dramatically increased from ∼0.50 to 0.75 with particle density changes from 5 to 250 particles /μm^3, while the change of photocurrent from AuNRs was from 0.47 to 0.48 with a similar range of particle density change in AuNPs.

Next, we turned to performing rapid detection of cytokine with our devices. Our study employed interleukin-1 beta (IL-1β), a pro-inflammatory cytokine, in an aqueous phase as our model analyte. We chose IL-1β as the target because of (i) its clinical significance in immune monitoring processes,[36] (ii) the well-established binding chemistry between IL-1β and its antibody on AuNPs (Figure 1),[16−18,37−39] and (iii) its surface binding that causes a near-field refractive index change without causing optical interference.[40−42] The biosensor preparation involved: (i) immobilization of AuNPs onto a SiO_2 thin layer

DOI: 10.1021/acsnano.7b01162
ACS Nano 2017, 11, 5697−5705

($AuNPs/SiO_2$), (ii) self-assembly of 1-ethyl-3-[3-(dimethylamino)propyl] carbodiimide (EDC) and *N*-hydroxysuccinimide (NHS) on the particle surfaces, (iii) antibody conjugation on the functionalized particles ($Ab\text{-}AuNP/SiO_2$), and (iv) attachment of the $Ab\text{-}AuNP/SiO_2$ thin layer on a few-layer MoS_2 flake with an alignment mark. The Ab-AuNP conjugate (50 nm in diameter) scatters light at λ = 532 nm with a sufficient intensity. The measured photocurrent (I_{ds}) increases over time with cytokine-antibody binding progressing on a nanoparticle surface. Here, a local refractive index change accompanying the cytokine binding causes a red shift of the extinction peak of the particle, leading to higher light transmission through the nanoplasmonic filter (Figure 3a). After loading IL-1β ($C_{IL\text{-}1\beta}$ = 10 pg/mL) in a phosphate-buffered saline (PBS) solution followed by a 30 min incubation process, the photoresponse of the device to a light illumination was measured as a function of time (Figure 3b). At t = 0 min, the photocurrent I_{ds} was ~0.11 μA at V_{ds} = 1.0 V. The I_{ds} at V_{ds} = 1.0 V increased two times to ~0.23 μA in 10 min during the incubation process and reached a plateau later with the IL-1β-anti-IL-1β binding equilibrium established on the AuNPs of the nanoplasmonic filter. The plot of I_{ds} over time (I_{ds}–time curve) represents the IL-1β binding kinetics and allows us to estimate the binding affinity of IL-1β. The attachment and detachment rates of IL-1β were obtained from curve fitting to the plot based on a standard 1:1 binding kinetics model as $k_{off} = 4.2 \times 10^{-5}$ M^{-1} s^{-1} and $k_{on} = 2.9 \times 10^{5}$ M^{-1} s^{-1}, respectively. The equilibrium constant (K_{eq}) was estimated to be 6.9×10^{9} M^{-1}, which well matches a typical equilibrium constant value for an antigen–antibody interaction. With five repeats of the measurement (Figure S4), we observed good repeatability of the biosensing performance of the device. In addition, we would expect a shorter detection time to determine the concentration of IL-1β using our subthreshold regimes analysis in the few-layer MoS_2 thin-film transistors.[28] The I_{ds} variation ($\Delta I_{ds}/I_o$)–time curves with a light illumination reached a steady state in ~10 min (Figure 3c). Both at V_{ds} = 1.0 and −1.0 V, the time for the steady state is similar. Regardless of V_{ds} = 1.0 and −1.0 V, the $\Delta I_{ds}/I_o$ shows a consistent value (= 0.8) at the steady state.

We further performed the cytokine measurement with different concentrations of IL-1β from 0.1pg/mL to 1 ng/mL (Figure 4). Varying the concentration of IL-1β is expected to change the overlapping spectral band between the extinction peak of the nanoparticle and the wavelength of the light source. Increasing the IL-1β concentration results in higher optical transmission, leading to an increase in the photocurrent of the device (Figure 4a). Measuring the photocurrent changes allowed us to quantify the IL-1β concentration of a sample. Our biosensor device incorporating the high-sensitivity few-layer MoS_2 photoconductive thin layer enabled recognition of a very low light intensity change at the presence of low-concentration IL-1β. We first measured the LSPR extinction spectral peak shift of the anti-$AuNP/SiO_2$ thin layer from $C_{IL\text{-}1\beta}$ = 0.1 pg/mL to 1 ng/mL using a photospectrometer (USB4000, Ocean Optics).[17,18] The measured peak shift was ~0 or 0.2 nm (Figure 4b), which was too small to detect with the above-mentioned LSPR extinction spectrum detection setup, whereas our device allowed quantification of IL-1β at a low concentration by managing to detect the subtle LSPR peak shift. At V_{ds} = 1 V, I_{ds} increases from ~0.15 μA to 0.45 μA with $C_{IL\text{-}1\beta}$ increasing from 0.1 pg/mL to 1 ng/mL. The I_{ds}–time curves across the measured range of $C_{IL\text{-}1\beta}$ reached a steady state in ~10 min as we observed in Figure 3c. Figure 4c represents the standard curve of our device and clearly demonstrates that the device yields high cytokine detection sensitivity and a large (10^6) dynamic range. We compared sensitivity between our biosensor ($LSPR/MoS_2$) and the commercial photospectrometer detecting an extinction spectral shift (LSPR) at the same surface density of AuNP on SiO_2 as a function of IL-1β concentration. In the comparison, we determined the limit of detection from the decoupled LSPR/MoS_2 (LOD_{LSPR/MoS_2}) from the obtained calibration curve (Figure 4d). Our device achieved a LOD_{LSPR/MoS_2} of 0.25 pg/mL, while the direct LSPR extinction peak shift detection obtained a LOD_{LSPR} of 22.5 pg/mL at the same density of AuNPs. Here, all the LOD values were given by $3\sigma/k_{slope}$, where σ and k_{slope} are the standard deviation of background signal measured from a blank control and regression slope of calibration curve, respectively. Our method is ~90 times more sensitive than the common LSPR peak shift detection method. The LOD_{LSPR/MoS_2} was also compared to the LOD obtained from ELISA, which is the current gold standard immunoassay method (Table S2). In addition, the selectivity of the $LSPR/MoS_2$ biosensor was explored by testing the device response to four relevant cytokines, including tumor necrosis factor (TNF)-α, interferon type (INF)-γ, IL-6, and IL-1β at a concentration range from 0.1 to 100 pg/mL (Figure S5). We observed no variations of I_{ds} with analyte concentration for other cytokines than IL-1β. This verifies that the cross-reactivity is negligible with our device.

CONCLUSIONS

We have successfully developed a high-sensitivity, label-free cytokine immunobiosensing device integrating AuNP plasmonic biosensing assemblies on a SiO_2 thin layer and a MoS_2 photoconductive flake. The binding of biomolecules at the surfaces of antibody-conjugated AuNPs changed the extinction spectrum peak of the SiO_2 thin layer due to a LSPR peak shift between AuNPs and incident light. We showed that this effect enabled the $AuNP\text{-}SiO_2$ thin layer to act as a tunable optical filter responding to the presence of cytokines in a solution deposited on the device surface. The decoupled device architecture prevented electronic interactions between the photoexcited AuNP assemblies and semiconducting MoS_2 with a physical gap. This arrangement enabled highly stable detection of subtle variations of photocurrent in the MoS_2 layer accompanying changes in the light transmission of the $AuNP\text{-}SiO_2$ film during biomolecule quantification in an aqueous solution. As a result, we were able to detect IL-1β in PBS at a concentration as low as 250 fg/mL (14 fM) while obtaining its surface binding curve. The demonstrated dynamic range was as large as 10^6, which is about 2 orders of magnitude larger than that of ELISA. Real-time monitoring of the binding curve enabled us to complete the analysis within 10 min without waiting for the biosensing process to reach an equilibrium state, which is at least ~50 times faster than gold standard assays. The plasmo-photoelectronic biomolecule detection approach demonstrated in this study makes our device highly poised for standalone operation with its monolithically integrated architecture eliminating the need for an external signal reader, which would reveal a future direction for clinically relevant point-of-care applications. All of these device features represent immunoassay performances superior to those of conventional ELISA-based techniques.

DOI: 10.1021/acsnano.7b01162
ACS Nano 2017, 11, 5697–5705

METHODS AND EXPERIMENTAL SECTION

Chemicals. Gold nanoparticle (gold nanosphere (AuNPs, d = 50 nm) and AuNRs (d_1/d_2 = 40/68 nm) were purchased from NanoSeedz. 3-Aminopropyl triethoxysilane (APTES), 10-carboxy-1-decanethiol (C-10), and albumin, from bovine serum (BSA), were purchased from Sigma-Aldrich. 1-Ethyl-3-[3-(dimethylamino)propyl] carbodiimide (EDC) and *N*-hydroxysuccinimide (NHS) were purchased from Thermo Co. Ltd. IL-1β and Anti IL-1β were purchased from Life Technologies, Frederick, MD. Polydimethylsiloxane (PDMS) elastomer and curing agent were purchased from Coring. Nanopure deionized (DI) water (18.1 MΩ·cm) was produced in-house.

Nanoplasmonic Filter. *Plasmonic Structure.* To prepare the gold nanostructure, we centrifuged AuNP and AuNR stock solutions (0.2 nM) three times at 5000 rpm for 10 min and washed them in DI water to remove excessive structure direction agents (citrate for AuNP and cetrimonium bromide (CTAB, cetyltrimethylammonium bromide) for AuNR) in the solutions. As a substrate, we used thin SiO_2 layer (100 μm). The SiO_2 substrate was rinsed with acetone, isopropanol, and DI water. Piranha clean with a solution of H_2SO_4:H_2O_2 = 3:1 v/v was followed for 30 min. The SiO_2 substrate was washed with DI water carefully. After drying, the surface of the SiO_2 substrate was treated by O_2 plasma for 2 min at 18 W (COVANCE 1-MP, Femto). Then a number of hydroxyl groups on the SiO_2 substrate could be created on the surface. Then the SiO_2 substrate was incubated in a 0.1 M APTES solution for 6 h. The AuNP (or AuNR) solution was then loaded into a chamber and incubated overnight. The inlets and outlets were sealed with a cover glass to prevent evaporation and avoid dry-out of the AuNP (or AuNR) solution during incubation. After the incubation, the AuNPs-SiO_2 (or AuNR-SiO_2) substrate was washed with DI water, and strong air blowing was followed.

Ab-AuNP. After preparing the AuNP (or AuNR) array on the SiO_2 substrate, we functionalized it with thiolated alkane 10-carboxy-1-decanethiol (HS-(CH_2)10-COOH) using a self-assembly method (SAM). At first, the SiO_2 substrate was incubated in 1 mM of HS-$(CH_2)_{10}$-COOH overnight. Then the formed carboxylic group (−COOH) on the AuNP surface enabled us to attach a linker for antibody. The antibody linking was performed by way of the antibody binding to the −COOH functional group through standard EDC/NHS coupling chemistry. After washing the −COOH formed AuNP (or AuNR)-SiO_2 substrate, we loaded a mixture of 0.4 M EDC and 0.1 M NHS at a 1:1 volume ratio in a 0.1 M EDC solution into the chamber to activate the AuNP (or AuNR) array surfaces on the SiO_2 substrate. Then, to attach the antibody, we prepared diluted primary cytokine antibodies from 100 to 10 μg/mL in 1 × PBS. We loaded the prepared antibody solution into the chamber and incubated it at room temperature for 60 min. To suppress the nonspecific binding on the detection surface, we treated the prepared anti-AuNP (or anti-AuNR) conjugates with 10 μL of 1% BSA in 1 × PBS in blocking buffer and incubated the whole system for 20 min. Before detecting cytokines, the anti-AuNP (or anti-AuNR) array surface was thoroughly washed to remove any excessive solutions or molecules using 20 μL of 1 × PBS.

Highly Sensitive Few-Layer MoS_2 Photodetector. *Fabrication and Characterization of MoS_2 Biosensors (Figure S6).* We fabricated the few-layer MoS_2 thin-film transistors using a micro printing method.[34] Flake MoS_2 channel thicknesses were specifically controlled to be 15−20 nm. Such a MoS_2 thickness range has been demonstrated to result in the optimal field-effect mobility values for MoS_2 transistors. The transistor channel lengths (L) were ∼10 μm and the channel widths (W) ranged from 5 μm. Ti (5 nm)/Au (50 nm) electrode pairs served as drain (D) and source (S) contacts, which were created using photolithography followed by metal deposition and lift-off. Such thin SiO_2 layers can enable a simple color coding method whereby MoS_2 flakes with suitable thicknesses (*i.e.*, 15−20 nm) may be quickly identified.

Integration of Nanoplasmonic Filter and a Few-Layer MoS_2 Photodetector Device. After separately preparing a AuNP/SiO_2 nanoplasmonic optical filter thin layer and an atomically layered MoS_2 photodetector, we assembled them into the same device platform. Using macromanipulation control, we placed the AuNP/SiO_2 on Au electrode of MoS_2 detection platform. Along the alignment marks in both SiO_2 substrates of Au/SiO_2 and MoS_2/SiO_2, we made a constant location between nanoplasmonic filter and MoS_2 photodetector. To avoid any alignment change, the nanoplasmonic optical filter and MoS_2 photodetector were physically bonded using a dielectric sticky PDMS thin (0.5 mm) handling layer.

Photocurrent Measurement. All electrical measurements were performed using an HP-4145B semiconductor parameter analyzer. A 532 nm laser (power density, 5 mW/cm^2) was also employed to characterize the PV response performance of the devices under light illumination. Even though sensitivity is lower than that of the MoS_2 photodetector, as a reference, power density through the plasmonic nanofilter was also confirmed by a conventional power meter (Newport, 843-R) (Figure S7).

LSPR Peak Shift Measurement Protocol. The fabricated and prepared LSPR biosensor microarray chip was mounted on a motorized stage (ProScan, Prior Scientific) to position the on chip sensing spot at ease and to automate the signal scanning. A dark-field condenser (NA = 1.45, MBL12000, Nikon) was closely placed to the backside of the glass substrate (the opposite side of the AuNPs (or AuNRs)-deposited sensor side) using lens oil. The light scattered from the AuNR nanoplasmonic biosensor arrays was collected using a 20× objective lens under the chip. The spectrum was collected by a spectrometer (Ocean optics, USB 4000).

Calculation of Electric Field. We simulated near-field electromagnetic fields around AuNP and AuNR using a finite element analysis (FEA, COMSOL Multiphysics software) solving Helmholtz wave equation: $\nabla \times (\mu_r^{-1}\nabla \times E) - k_0^2 (\varepsilon_r - j\sigma\omega\varepsilon_0)$, $E = 0$. Hybrid mesh structures were created for the AuNP and the AuNR to adapt their round shape. We assumed the relative permeability and complex permittivity of gold to be $\mu_r = 1$ and $\varepsilon_r = f(\lambda)$, respectively. The polarization vector was applied in the direction parallel to the AuNR structure, whereas the direction of the **k**-vector was taken to be perpendicular to the plane of the structure. Assuming perfect absorption at the outer boundary, we put a perfectly matched layer and an integration layer in concentric space to minimize spurious reflections. The dimensions of the AuNP (d = 50 nm) and the AuNR (d = 40 nm and l = 68 nm) were chosen based on the SEM images as shown in Figure 2. The surface plasmon of the AuNP is strongly excited at λ = 532 nm, while the AuNR shows weak excitation at the same wavelength. The adaptive mesh was refined until the maximum electric field converged. Primarily, FEA was used, owing to its ability to produce adaptive meshes with high flexibility in geometry. It is more practical than the finite difference time domain (FDTD) method for the complex geometry studied here.

ASSOCIATED CONTENT

Supporting Information

The Supporting Information is available free of charge on the ACS Publications website at DOI: 10.1021/acsnano.7b01162.

Spectral response of the few-layer MoS_2 photoconductive flake; morphologies of plasmonic nanoprobes of AuNPs and AuNRs; optical properties of nanoplasmonic optical filter; I_{ds} *vs* V_{ds} curve as a function of time with varying $C_{IL\text{-}1\beta}$; highly selective detection of IL-1β; schematics of device design and optical setup of integrated device; power density measurement; comparison of photoresponsivity of MoS_2-based photodetectors; LOD resulting from different cytokine detection methods (PDF)

AUTHOR INFORMATION

Corresponding Authors

*E-mail: katsuo@umich.edu.
*E-mail: xiaoganl@umich.edu.

DOI: 10.1021/acsnano.7b01162
ACS Nano 2017, 11, 5697−5705

ORCID

Xiaogan Liang: 0000-0002-7390-9130
Katsuo Kurabayashi: 0000-0002-9613-3590

Author Contributions

[§]Y.P. and B. R. contributed equally.

Notes

The authors declare no competing financial interest.

ACKNOWLEDGMENTS

This research was supported by academic research fund at University of Michigan and the National Science Foundation (CBET1263889).

REFERENCES

(1) Dinarello, C. A. Historical Insights into Cytokines. *Eur. J. Immunol.* **2007**, *37*, S34−S45.
(2) Meager, T. *The Molecular Biology of Cytokines*; Wiley: New York, 1998.
(3) Thompson, A. W.; Lotze, M. T. *The Cytokine Handbook*, 4th ed.; Academic Press: Amsterdam, Netherlands, 2003.
(4) Bienvenu, J.; Monneret, G.; Fabien, N.; Revillard, J. P. The Clinical Usefulness of the Measurement of Cytokines. *Clin. Chem. Lab. Med.* **2000**, *38*, 267−285.
(5) Payen, D.; Monneret, G.; Hotchkiss, R. Immunotherapy - A Potential New WayForward in the Treatment of Sepsis. *Crit. Care* **2013**, *17*, 118.
(6) Rosenberg, S. A.; Yang, J. C.; Restifo, N. P. Cancer Immunotherapy: Moving Beyond Current Vaccines. *Nat. Med.* **2004**, *10*, 909−915.
(7) Ludewig, B.; Ochsenbein, A. F.; Odermatt, B.; Paulin, D.; Hengartner, H.; Zinkernagel, R. M. Immunotherapy with Dendritic Cells Directed Against Tumor Antigens Shared with Normal Host Cells Results in Severe Autoimmune Disease. *J. Exp. Med.* **2000**, *191*, 795−803.
(8) Valenta, R. The Future of Antigen-Specific Immunotherapy of Allergy. *Nat. Rev. Immunol.* **2002**, *2*, 446−453.
(9) Siebert, S.; Tsoukas, A.; Robertson, J.; McInnes, I. Cytokines as Therapeutic Targets in Rheumatoid Arthritis and Other Inflammatory Diseases. *Pharmacol. Rev.* **2015**, *67*, 280−309.
(10) Targan, S. R.; Hanauer, S. B.; vanDeventer, S. J. H.; Mayer, L.; Present, D. H.; Braakman, T.; DeWoody, K. L.; Schaible, T. F.; Rutgeerts, P. J. A Short-Term Study of Chimeric Monoclonal Antibody cA2 to Tumor Necrosis Factor Alpha for Crohn's Disease. *N. Engl. J. Med.* **1997**, *337*, 1029−1035.
(11) Abraham, E. Why Immunomodulatory Therapies Have Not Worked in Sepsis. *Intensive Care Med.* **1999**, *25*, 556−566.
(12) Fink, M. P.; Warren, H. S. Strategies to Improve Drug Development for Sepsis. *Nat. Rev. Drug Discovery* **2014**, *13*, 741−758.
(13) Kox, W. J.; Volk, T.; Kox, S. N.; Volk, H.-D. Immunomodulatory Therapies in Sepsis. *Intensive Care Med.* **2000**, *26*, S124−S128.
(14) Osuchowski, M. F.; Connett, J.; Welch, K.; Granger, J.; Remick, D. G. Stratification is the Key: Inflammatory Biomarkers Accurately Direct Immunomodulatory Therapy in Experimental Sepsis. *Crit. Care Med.* **2009**, *37*, 1567−1573.
(15) Wong, H. R.; Weiss, S. L.; Giuliano, J. S.; Wainwright, M. S.; Cvijanovich, N. Z.; Thomas, N. J.; Allen, G. L.; Anas, N.; Bigham, M. T.; Hall, M.; Freishtal, R. J.; Sen, A.; Meyer, K.; Checchia, P. A.; Shanley, T. P.; Nowak, J.; Quasney, M.; Chopra, A.; Fitzgerald, J. C.; Gedeit, R. Testing the Prognostic Accuracy of the Updated Pediatric Sepsis Biomarker Risk Model. *PLoS One* **2014**, *9*, e86242.
(16) Chen, P.; Chung, M. T.; McHugh, W.; Nidetz, R.; Li, Y.; Fu, J.; Cornell, T. T.; Shanley, T. P.; Kurabayashi, K. Multiplex Serum Cytokine Immunoassay Using Nanoplasmonic Biosensor Microarrays. *ACS Nano* **2015**, *9*, 4173−4181.
(17) Oh, B.-R.; Chen, P.; Nidetz, R.; McHugh, W.; Fu, J.; Shanley, T. P.; Cornell, T. T.; Kurabayashi, K. Multiplexed Nanoplasmonic Temporal Profiling of T-Cell Response under Immunomodulatory Agent Exposure. *ACS Sens.* **2016**, *1*, 941−948.
(18) Oh, B.-R.; Huang, N.-T.; Chen, W.; Seo, J. H.; Chen, P.; Cornell, T. T.; Shanley, T. P.; Fu, J.; Kurabayashi, K. Integrated Nanoplasmonic Sensing for Cellular Functional Immunoanalysis Using Human Blood. *ACS Nano* **2014**, *8*, 2667−2676.
(19) De La Rica, R.; Stevens, M. M. Plasmonic ELISA for the Ultrasensitive Detection of Disease Biomarkers with the Naked Eye. *Nat. Nanotechnol.* **2012**, *7*, 821−824.
(20) Qu, Z.; Xu, H.; Xu, P.; Chen, K.; Mu, R.; Fu, J.; Gu, H. Ultrasensitive ELISA using Enzyme-Loaded Nanospherical Brushes as Labels. *Anal. Chem.* **2014**, *86*, 9367−9371.
(21) Tekin, H. C.; Gijs, M. A. Ultrasensitive Protein Detection: a Case for Microfluidic Magnetic Bead-Based Assays. *Lab Chip* **2013**, *13*, 4711−4739.
(22) Ghatak, S.; Pal, A. N.; Ghosh, A. Nature of Electronic States in Atomically Thin MoS_2 Field-Effect Transistors. *ACS Nano* **2011**, *5*, 7707−7712.
(23) Fuhrer, M. S.; Hone, J. Measurement of Mobility in Dual-Gated MoS_2 Transistors. *Nat. Nanotechnol.* **2013**, *8*, 146−147.
(24) Radisavljevic, B.; Radenovic, A.; Brivio, J.; Giacometti, i. V.; Kis, A. Single-Layer MoS_2 Transistors. *Nat. Nanotechnol.* **2011**, *6*, 147−150.
(25) Tsai, D.-S.; Liu, K.-K.; Lien, D.-H.; Tsai, M.-L.; Kang, C.-F.; Lin, C.-A.; Li, L.-J.; He, J.-H. Few-layer MoS_2 with High Broadband Photogain and Fast Optical Switching for Use in Harsh Environments. *ACS Nano* **2013**, *7*, 3905−3911.
(26) Xiao, D.; Liu, G.-B.; Feng, W.; Xu, X.; Yao, W. Coupled Spin and Valley Physics in Monolayers of MoS_2 and Other Group-VI Dichalcogenides. *Phys. Rev. Lett.* **2012**, *108*, 196802.
(27) Nam, H.; Oh, B.-R.; Chen, M.; Wi, S.; Li, D.; Kurabayashi, K.; Liang, X. Fabrication and Comparison of MoS_2 and WSe_2 Field-Effect Transistor Biosensors. *J. Vac. Sci. Technol., B: Nanotechnol. Microelectron.: Mater., Process., Meas., Phenom.* **2015**, *33*, 06FG01.
(28) Nam, H.; Oh, B.-R.; Chen, P.; Chen, M.; Wi, S.; Wan, W.; Kurabayashi, K.; Liang, X. Multiple MoS_2 Transistors for Sensing Molecule Interaction Kinetics. *Sci. Rep.* **2015**, *5*, 10546−10546.
(29) Liu, M.; Yin, X.; Zhang, X. Double-Layer Graphene Optical Modulator. *Nano Lett.* **2012**, *12*, 1482−1485.
(30) Miao, J.; Hu, W.; Jing, Y.; Luo, W.; Liao, L.; Pan, A.; Wu, S.; Cheng, J.; Chen, X.; Lu, W. Surface Plasmon-Enhanced Photodetection in Few Layer MoS_2 Phototransistors with Au Nanostructure Arrays. *Small* **2015**, *11*, 2392−2398.
(31) Su, S.; Sun, H.; Cao, W.; Chao, J.; Peng, H.; Zuo, X.; Yuwen, L.; Fan, C.; Wang, L. Dual-Target Electrochemical Biosensing Based on DNA Structural Switching on Gold Nanoparticle-Decorated MoS_2 Nanosheets. *ACS Appl. Mater. Interfaces* **2016**, *8*, 6826−6833.
(32) Sun, H.; Chao, J.; Zuo, X.; Su, S.; Liu, X.; Yuwen, L.; Fan, C.; Wang, L. Gold Nanoparticle-Decorated MoS_2 Nanosheets for Simultaneous Detection of Ascorbic Acid, Dopamine and Uric Acid. *RSC Adv.* **2014**, *4*, 27625−27629.
(33) Lopez-Sanchez, O.; Lembke, D.; Kayci, M.; Radenovic, A.; Kis, A. Ultrasensitive Photodetectors Based on Monolayer MoS_2. *Nat. Nanotechnol.* **2013**, *8*, 497−501.
(34) Nam, H.; Wi, S.; Rokni, H.; Chen, M.; Priessnitz, G.; Lu, W.; Liang, X. MoS_2 Transistors Fabricated *via* Plasma-Assisted Nanoprinting of Few-layer MoS_2 Flakes into Large-Area Arrays. *ACS Nano* **2013**, *7*, 5870−5881.
(35) Alicea, J.; Oreg, Y.; Refael, G.; von Oppen, F.; Fisher, M. P. Non-Abelian Statistics and Topological Quantum Information Processing in 1D Wire Networks. *Nat. Phys.* **2011**, *7*, 412−417.
(36) Masters, S. L.; Simon, A.; Aksentijevich, I.; Kastner, D. L. Horror Autoinflammaticus: the Molecular Pathophysiology of Autoinflammatory Disease. *Annu. Rev. Immunol.* **2009**, *27*, 621.
(37) Dondapati, S. K.; Sau, T. K.; Hrelescu, C.; Klar, T. A.; Stefani, F. D.; Feldmann, J. Label-Free Biosensing Based on Single Gold Nanostars as Plasmonic Transducers. *ACS Nano* **2010**, *4*, 6318−6322.
(38) Mayer, K. M.; Lee, S.; Liao, H.; Rostro, B. C.; Fuentes, A.; Scully, P. T.; Nehl, C. L.; Hafner, J. H. A Label-Free Immunoassay

DOI: 10.1021/acsnano.7b01162
ACS Nano 2017, 11, 5697−5705

Based Upon Localized Surface Plasmon Resonance of Gold Nanorods. *ACS Nano* **2008**, *2*, 687−692.
(39) Wang, X.; Li, Y.; Wang, H.; Fu, Q.; Peng, J.; Wang, Y.; Du, J.; Zhou, Y.; Zhan, L. Gold Nanorod-Based Localized Surface Plasmon Resonance Biosensor for Sensitive Detection of Hepatitis B Virus in Buffer, Blood Serum and Plasma. *Biosens. Bioelectron.* **2010**, *26*, 404−410.
(40) Haes, A. J.; Van Duyne, R. P. A Nanoscale Optical Biosensor: Sensitivity and Selectivity of an Approach Based on the Localized Surface Plasmon Resonance Spectroscopy of Triangular Silver Nanoparticles. *J. Am. Chem. Soc.* **2002**, *124*, 10596−10604.
(41) Jung, L. S.; Campbell, C. T.; Chinowsky, T. M.; Mar, M. N.; Yee, S. S. Quantitative Interpretation of the Response of Surface Plasmon Resonance Sensors to Adsorbed Films. *Langmuir* **1998**, *14*, 5636−5648.
(42) Willets, K. A.; Van Duyne, R. P. Localized Surface Plasmon Resonance Spectroscopy and Sensing. *Annu. Rev. Phys. Chem.* **2007**, *58*, 267−297.

DOI: 10.1021/acsnano.7b01162
ACS Nano 2017, 11, 5697−5705